ARID ZONE JOURNAL OF ENGINEERING, TECHNOLOGY & ENVIRONMENT
AZOJETE June 2024. Vol. 20(2):435-452
Published by the Faculty of Engineering, University of Maiduguri, Maiduguri, Nigeria.
Print ISSN: 1596-2490, Electronic ISSN: 2545-5818
www.azojete.com.ng

DEVELOPMENT AND SIMULATION OF A ROTOR FLUX- ORIENTED CONTROL SCHEME FOR EFFICIENCY IMPROVEMENT IN A THREE PHASE INDUCTION MOTOR

G. A. Olarinoye*, F.O. Balogun and A. S. Abubakar

Department of Electrical Engineering, Faculty of Engineering, Ahmadu Bello University, Zaria

**Corresponding author's email address: baolarinoye@abu.edu.ng*

ARTICLE INFORMATION

Submitted 23 March, 2023
Revised 23 December, 2023
Accepted 4 January, 2024

Keywords:
Flux control
PI controller
induction motor
efficiency
optimization
simulink

ABSTRACT

The efficiency of induction motor drives under variable operating load and speed conditions can be improved by developing an algorithm that compute the optimum flux in the motor and commands a voltage that drives the motor at maximum efficiency for any given load and speed. This approach also helps to achieve significant amount of savings in electric energy consumption. In this paper, a method to optimize the flux of a three-phase induction motor and thereby maximize its efficiency for each load torque applied at a given speed, was developed. Mathematical models for the conventional rotor flux-oriented control scheme, total power loss as a function of rotor flux and for optimum flux as a function of operating speed and load torque were analytically derived. A MATLAB/Simulink model of the proposed rotor flux optimization scheme was developed to verify the analyses set forth for a typical three-phase Induction Motor. The results of the proposed method were compared with those of the conventional rotor flux control method and direct torque control (DTC) method in terms of loss reduction and efficiency for the same induction motor. The proposed rotor flux optimization scheme achieved 8.51% improvement in efficiency compared to the conventional rotor flux control scheme at a speed of 250 rad/s for a load torque of 3Nm. It also achieved 5.01% improvement in efficiency compared to the optimized DTC control scheme for the same speed and load torque. At a lower speed of 150 rad/s, power loss reduced by 17.1% while efficiency was higher by 5.7% for a load torque of 3Nm under the proposed scheme as compared to the optimized DTC scheme.

1.0 Introduction

Induction motors are the most widely used electric machine in the industry because of their ruggedness, cheapness and very low maintenance cost. Studies have shown that bulk of the energy used in the industry is consumed, largely, by induction motors (Engel *et al.,*2015). Therefore, efforts have been made over the years by various manufacturers of induction motors in the technique of construction of Energy Efficient Motors (EEM). This has resulted in significant improvements in efficiency and increase in energy savings. Induction motor have high efficiency at rated speed and torque, but the efficiency of induction motor decreases greatly at light loads because of an imbalance in copper and core losses. Energy saving can however, be achieved by proper selection of the flux level in the motor (Eseosa and Christian, 2018). Losses in the induction motor are classified into stator copper losses, rotor copper losses, core losses, stray losses, friction and windage losses. The copper and core losses account for the largest amount of losses in induction motor and therefore explain the interest to use them in the analysis proposed in this paper. In order to increase the motor efficiency, the flux must be

reduced and balance obtained between copper and core losses. Basically, there are two approaches to improving the efficiency of induction motor (Faduyile, 2009). These are the Loss-based model approach and the Power measure-based approach. In the loss-based model approach, the model-based controller computes losses by using the machine model and thereby determines a flux level that minimizes the losses. This approach is fast and does not produce torque ripple. In the power measure-based approach, the controller searches for the operating points where the output power is constant (Rashtchi and Bizhani, 2015).

In this paper, Loss-based model approach or Loss model controller of induction motor drive system that determines the optimal flux for loss minimization was analysed and implemented in MATLAB/Simulink. The significance of the method applied in this paper is the reduction in energy consumed by the induction motor for the same load torque over the period of motor operation. The benefit is that it will go a long way to reduce operating cost and to make spare energy available to meet other energy demands. In the long term, this benefit should also slow the world's overall energy consumption and protect the environment from pollution and preserve the world natural resources from further depletion.

Induction motors are large consumers of the electric energy, and are designed to operate efficiently at rated loads. Unfortunately, these motors operate on partial or low loads most of the time and this situation leads to inefficient motor operation with attendant losses in energy and increased operating cost. The proposed work seeks to reduce the inefficiency of Induction motor operation under the conditions of partial or low load operation by developing a method to maximize the efficiency of the motor under these conditions.

Several papers relating to loss minimization in Induction motors have been published in recent times. Rashtchi and Bizhani (2015) presented a new online loss minimization algorithm using particle swam optimization (PSO) to determine the optimum flux level for the efficiency optimization of vector-controlled induction motor. Khan *et al.* (2015) developed a high performance and robust control structure called the flux optimized direct torque control for induction motor. Lee *et al.* (2013) presented a loss based model controller using a digital signal processor (TM320LF2812), for Induction motor efficiency maximization and energy saving**.** Sruthi *et al.* (2017) formulated a loss minimization algorithm for energy saving and efficiency improvement in induction motor drive. The input voltage and frequency were optimized to reduce total losses. Eseosa & Christian (2018), Afify *et al.* (2018), Chelliah (2009), Nam and Uddin (2006) and Laroui, *et al.* (2021) presented various approaches in optimization control techniques to improve the efficiency operation of induction motor. Aygun and Aktas (2018) implemented a DTC technique combined with an online loss minimization model-based controller to minimize the losses of an induction motor applied in Electric Vehicle (EV).

The aim of this paper is to develop a rotor flux optimization control model for an existing induction motor and simulate its performances in MATLAB/Simulink for loss minimization and efficiency improvement.

2.0 Material and Methods

This section presents the model of the three-phase induction motor. The model was developed into a rotor flux-oriented control scheme and subsequently, a flux optimization control algorithm was developed and implemented in MATLAB/Simulink to minimize losses and therefore maximize motor efficiency.

2.1 Mathematical Model of Three Phase Induction Motor

The dynamic model of the induction motor in *d-q* coordinates established in a rotor flux-oriented reference frame is provided in equations (1) – (10) (Kalhoodashti and Shahbazian, 2011).

$$V_{qs} = R_s i_{qs} + \omega_e \lambda_{ds} + p\lambda_{qs} \quad (1)$$

Corresponding author's e-mail address: baolarinoye@abu.edu.ng

$$V_{ds} = R_s i_{ds} - \omega_e \lambda_{qs} + p\lambda_{ds} \quad (2)$$

$$V_{qr}^{'} = r_r^{'} i_{qr}^{'} + (\omega_e - \omega_r)\lambda_{dr}^{'} + p\lambda_{qr}^{'} \quad (3)$$

$$V_{dr}^{'} = r_r^{'} i_{dr}^{'} - (\omega_e - \omega_r)\lambda_{qr}^{'} + p\lambda_{dr}^{'} \quad (4)$$

$$\lambda_{qs} = (L_m + L_{ls}) i_{qs} + L_m i_{qr}^{'} \quad (5)$$

$$\lambda_{ds} = (L_m + L_{ls}) i_{ds} + L_m i_{dr}^{'} \quad (6)$$

$$\lambda_{qr}^{'} = L_m i_{qs} + (L_m + L_{lr}^{'}) i_{qr}^{'} \quad (7)$$

$$\lambda_{dr}^{'} = L_m i_{ds} + (L_m + L_{lr}^{'}) i_{dr}^{'} \quad (8)$$

$$T_e = \frac{3P}{4} \frac{L_m}{L_r^{'}} (\lambda_{dr}^{'} i_{qs} - \lambda_{qr}^{'} i_{qs}) \quad (9)$$

$$T_e = \frac{2}{p} Jp\omega_r + T_L \quad (10)$$

Where V_{ds} and V_{qs}, V_{dr} and V_{qr} are the direct axes and quadrature axes stator and rotor voltages, and i_{ds},i_{qs}, i_{dr} and i_{qr} are stator and rotor *d-q* currents, λ_{ds},λ_{qs}, λ_{dr} and λ_{qr} are the *d-q* stator and rotor flux respectively. R_s and $r_r^{'}$ are stator and rotor resistances respectively. ω_e is stator frequency and ω_r is the rotor electrical speed.

The equivalent circuit obtained from the mathematical model equations (1) - (8) of the Induction motor is shown in Figure 1

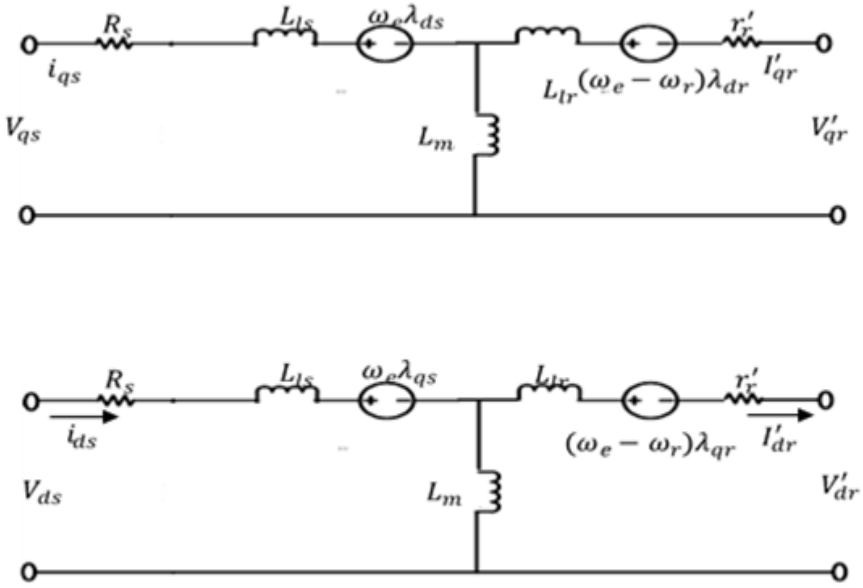

Figure 1: *q-d* axes equivalent circuit of the induction motor.

2.2 Rotor flux-oriented control scheme for the three-phase induction motor

The scheme is derived from the rotor dynamic equations of the three-phase induction machine in the synchronously rotating reference frame represented by equations (3)-(4) and (7)-(8).

The *q*-axis component of the rotor flux space vector $\lambda_{qr}^{'e}$ is equated to zero because of the alignment of the *d*-axis with the rotor flux vector (Olarinoye *et al*., 2022). It is mathematically represented as follows;

$$\lambda_{qr}^{'e} = 0 \quad (11)$$

The *d*-axis component of the rotor flux space vector $\lambda_{dr}^{'e}$ is now equal to the rotor flux magnitude $\lambda_r^{'e}$. The rotor flux magnitude is expressed as follows;

$$\lambda_r^{'e} = \sqrt{\lambda_{qr}^{'e^2} + \lambda_{dr}^{'e^2}} \quad (12)$$

Corresponding author's e-mail address: baolarinoye@abu.edu.ng

Mathematically, applying equations (11) to equations (12), (3)-(4), (7) and (8) yields the following results;

$$\lambda_r^{'e} = \lambda_{dr}^{'e} \quad (13)$$

$$0 = r_r' l_{qr}^{'e} + (w_e - w_r)\lambda_r^{e'} \quad (14)$$

$$0 = r l_{dr}^{'e} + \rho\lambda_{dr}^{e'} \quad (15)$$

$$\lambda_r^{e\prime} = L_m l_{ds}^{'} + L_r l_{dr}^{e} \quad (16)$$

$$0 = L_m l_{qs}^{e} + L_r l_{qr}^{\prime} \quad (17)$$

Equations (13) and (14) have been obtained considering that the short-circuited squirrel cage rotor of the three-phase induction motor have zero voltages in the q and d axis of the rotor windings

i.e. $V_{qr}^{e'} = 0$ and $V_{dr}^{e'} = 0$.

The rotor flux dynamics is developed from equations (15) and (16) to give the following;

$$\frac{\tau_r d\lambda_r^{e\prime}}{dt} + \lambda_r^{e'} = L_m l_{ds} \quad (18)$$

where $\tau_r = \frac{L_r}{r_r'}$ (19)

Equation (18) is a first order system governed by rotor time constant τ_r. The Slip frequency ω_s is obtained from equations (14) and (17) as follows;

$$w_s = w_e - w_r = \frac{R_r' L_m l_{qs}^{e}}{L_r' \lambda_r^{e\prime}} \quad (20)$$

The rotor flux angle θ_e, which is also the angle of transformation because of alignment of the d-axis to the rotor flux vector, is estimated by integrating the rotor flux angular frequency as follows

$$\theta_e = \int \omega_e \, dt = \int \left(\omega_r + \frac{r_r' L_m l_{qs}^{e}}{L_r' \lambda_r^{e\prime}}\right) dt \quad (21)$$

The torque produced in the three-phase induction motor given by equation (9) is modified, upon application of equations (11) and (13), to the following;

$$T_{em} = \frac{3P}{4}\frac{L_m}{L_r}\lambda_r^{'e} i_{qs}^{'e} \quad (22)$$

As a result of the alignment of the rotor flux magnitude with the *d*-axis, equations (18)-(21) enables the estimation of rotor flux magnitude and the phase angle or the angle of transformation.

2.3 Rotor flux optimization scheme

The objective of the flux optimization scheme is to regulate the flux magnitude such that minimum losses occur for a given load torque. The three-phase induction motor equivalent circuit was modified to account for the core loss resistance r_c. The equivalent circuit with core loss resistance is presented in Figure 2. As a result, the voltage, flux linkage and torque equations of the motor are reformulated to account for the effect of the core loss resistance.

Corresponding author's e-mail address: baolarinoye@abu.edu.ng

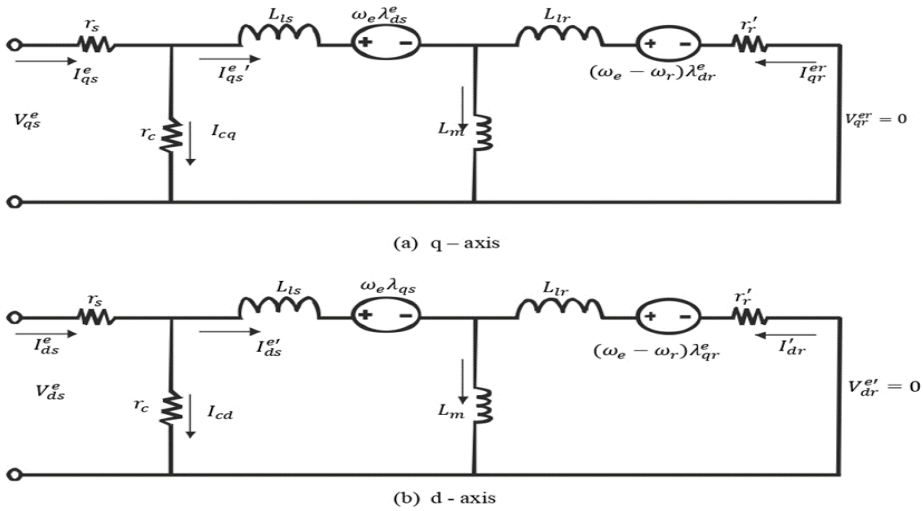

Figure 2: Three Phase Induction Motor *q-d* axis Equivalent Circuits accounting for Core Loss Resistance

The following voltage, flux linkage and current equations are derived from the equivalent circuits of Figures 2 (a) and (b) and equations (1)-(4) to give the following equations;

$$V^e_{qs} = R_s i^{e'}_{qs} + \mathrm{k}\omega_e\lambda^e_{ds} + kp\lambda^e_{qs} \tag{23}$$

$$V^e_{ds} = R_s i^{e'}_{ds} - \mathrm{k}\omega_e\lambda^e_{qs} + kp\lambda^e_{ds} \tag{24}$$

$$0 = r'_r i^{e'}_{qr} + (\omega_e - \omega_r)\lambda^{e'}_{dr} + p\lambda^{e'}_{qr} \tag{25}$$

$$0 = r'_r i^{e'}_{dr} - (\omega_e - \omega_r)\lambda^{e'}_{qr} + p\lambda^{e'}_{dr} \tag{26}$$

$$i_{cq} = i^e_{qs} - i^{e'}_{qs} \tag{27}$$

$$i_{cd} = i^e_{ds} - i^{e'}_{ds} \tag{28}$$

$$i_{cq} = \frac{V^e_{qs}}{kr_c} \tag{29}$$

$$i_{cd} = \frac{V^e_{ds}}{kr_c} \tag{30}$$

$$\text{Where } k = 1 + \frac{R_s}{r_c} \tag{31}$$

i_{cq} and i_{cd} are the currents flowing through the core loss branches of the *q* and *d* axes respectively. $i^{e'}_{qs}$ and $i^{e'}_{ds}$ are the torque currents responsible for producing electromagnetic torque in the motor as seen from the equivalent circuit of Figure 1.
By applying equations (11) and (13) to the voltage equations (23) – (26), relationships between the applied stator currents and torque currents were obtained as follows;

$$\begin{bmatrix} i_{qs} \\ i_{ds} \end{bmatrix} = \begin{bmatrix} \left(1 + \frac{R_s}{kr_c}\right) & \frac{\omega_e L_s}{r_c} \\ -\frac{\omega_e L_x}{r_c} & \left(1 + \frac{R_s}{kr_c}\right) \end{bmatrix} \begin{bmatrix} i'_{qs} \\ i'_{ds} \end{bmatrix} \tag{32}$$

Corresponding author's e-mail address: baolarinoye@abu.edu.ng

$$\begin{bmatrix} i'_{qs} \\ i'_{ds} \end{bmatrix} = \frac{1}{\left[1+\frac{R_s}{kr_c}\right]^2+\frac{\omega_e^2 L_x L_s}{r_c^2}} \begin{bmatrix} (1+\frac{R_s}{kr_c}) & -\frac{\omega_e L_s}{r_c} \\ \frac{\omega_e L_x}{r_c} & (1+\frac{R_s}{kr_c}) \end{bmatrix} \begin{bmatrix} i_{qs} \\ i_{ds} \end{bmatrix} \quad (33)$$

The power loss model was formulated considering that the total electrical power loss is the sum of the copper and core losses in the motor. The expression of electrical power loss is obtained from the equivalent circuits as follows;

$$P_L = R_s\left(i_{qs}^2 + i_{ds}^2\right) + r_r'\left(i_{qr}^2 + i_{dr}^2\right) + r_c\left(i_{cq}^2 + i_{cd}^2\right) \quad (34)$$

A power loss model was derived by substituting current equations (27) – (33) into equation (34). It is given as follows;

$$\mathrm{P_L} = \frac{3}{2}\left[\frac{2\mathrm{T_e^2 L_r^2}}{\mathrm{k_t^2 L_m^2 \lambda_r^2}} + \frac{2\lambda_r^2}{\mathrm{L_m^2}} - \frac{\mathrm{r_r}\lambda_r^2}{\mathrm{L_r^2}} + \mathrm{kL_m^2}\left(\frac{\mathrm{r_r^2 + L_r^2\omega_r^2}}{\mathrm{r_c L_r^4}}\right)\lambda_r^2 - 2\mathrm{k}\lambda_r^2\left(\frac{\mathrm{rr_r - \omega_e\omega_r LL_c}}{\mathrm{L_r^2 r_c}}\right) + \frac{2\mathrm{T_e}}{\mathrm{k_t r_c}}\left(\frac{\mathrm{k(\omega_e Lr_r + \omega_r rL_r)}}{\mathrm{L_r}} + \omega_e\right)\right] \quad (35)$$

The criterion for minimum loss is obtained by differentiating equation (35) with respect to the rotor flux magnitude as follows;

$$\frac{dP_L}{d\lambda_r} = \frac{3}{2}\left[\frac{-2Z\mathrm{T_e^2 L_r^2}}{\mathrm{k_t^2 L_m^2}\lambda_r^3} + \frac{2Z\lambda_r}{\mathrm{L_m^2}} - \frac{2\mathrm{r_r}\lambda_r}{\mathrm{L_r^2}} + 2\mathrm{kL_m^2}\left(\frac{\mathrm{r_r^2 + L_r^2\omega_r^2}}{\mathrm{r_c L_r^4}}\right)\lambda_r - 4\mathrm{k}\lambda_r\left(\frac{\mathrm{rr_r - \omega_e\omega_r LL_r}}{\mathrm{L_r^2 r_c}}\right)\right] = 0 \quad (36)$$

Equation (36) was solved to obtain the optimum value of rotor flux for minimum loss and hence maximum efficiency. The optimum value of the rotor $\lambda_{r(opt)}$ flux for a given load torque and speed was derived to yield;

$$\lambda_{\mathrm{r(opt)}} = \sqrt{\frac{\mathrm{T_e L_r^3}}{\mathrm{k_t}}} \cdot \sqrt[4]{\frac{\mathrm{Zr_c}}{\mathrm{kL_m^2(\omega_r^2 L_m^2 L_r^2 + 2\omega_e\omega_r LL_r^3 + L_m^2 r_r^2) + ZL_r^4 r_c - r_r L_r^2 r_c L_m^2 - 2krr_r L_r^2 L_m^2}}} \quad (37)$$

The efficiency of the induction motor was determined using the following equation;

$$\text{Efficiency} = \frac{Poweroutput}{Poweroutput + electricalpowerloss} \quad (38)$$

Equation (38) gives the efficiency as a function of electrical power loss in the machine.
For the purposes of controller design, the stator voltages are expressed as a function of the *d* and *q* axis currents and the rotor flux by applying equations (5) - (8), (11) and (13) to equations (23) and (24). The following expressions were obtained;

$$V_{qs}^e = kr_s' i_{qs}'^e + kLpi_{qs}'^e + k\omega_e L i_{ds}'^e + k\frac{L_m}{L_r}\omega_r \lambda_r'^e \quad (39)$$

$$V_{ds}^e = kr_s' i_{ds}'^e + kLpi_{ds}'^e - k\omega_e L i_{qs}'^e - k\frac{L_m}{L_r^2} r_r' \lambda_r'^e \quad (40)$$

Where:

$$L = L_s\left(1 - \frac{L_m^2}{L_s L_r}\right) \quad (41)$$

$$r_s' = R_s + \frac{L_m^2 r_r'}{L_r^2} \quad (42)$$

Equations (39) and (40) are first order non-linear systems for which V_{qs}^e and V_{ds}^e are inputs and $i_{qs}'^e$ and $i_{ds}'^e$ are outputs. The voltage commands needed to give the desired currents, $i_{qs}'^e$ and $i_{ds}'^e$, are obtained with a feedback-based solution using current controllers. The formulation

Corresponding author's e-mail address: baolarinoye@abu.edu.ng

for the controller gains was performed using equations (39) and (40) and illustrated in Figures 3 (a) and (b).

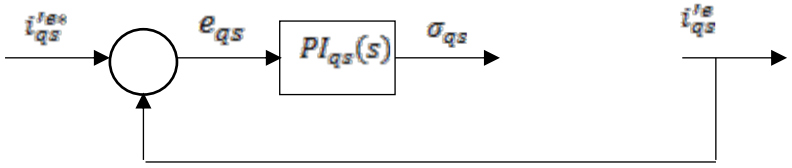

(a) q-axis current control

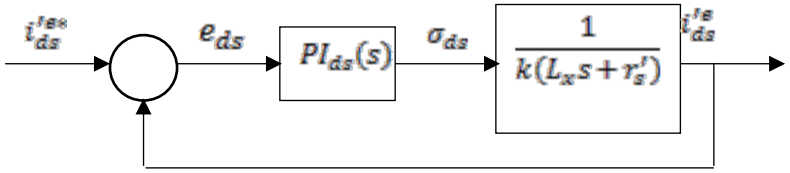

(b) d-axis current control

Figure 3: Control Block Diagram for Stator Current Control

σ_{qs} and σ_{ds} are defined as follows;

$$\sigma_{qs} = (r_s' + pL)ki_{qs}^{'e} \quad (43)$$

$$\sigma_{ds} = (r_s' + pL)ki_{ds}^{'e} \quad (44)$$

$PI_{qs}(s)$ and $PI_{ds}(s)$ are the *q* and *d* axis current PI controllers.

The closed loop transfer function of Figure 3 is defined as follows;

$$k(L_x s + r_s')i_s^{'e} = \left(k_p + \frac{k_i}{s}\right)(i_s^{'e*} - i_s^{'e}) \quad (45)$$

$$\frac{i_s^{'e}}{i_s^{'e*}} = \frac{sk_{pi}+k_{ii}}{s^2 kL + s(kr_s' + k_{pi}) + k_{ii}} \quad (46)$$

The expressions for the PI controller gains k_{pi} and k_{ii} were obtained by comparing the normalized denominator of equation (46) with the standard second order denominator, as follows;

$$s^2 + s\left(\frac{Kr_s' + k_{pi}}{KL}\right) + \frac{k_{ii}}{KL} \equiv s^2 + 2\zeta\omega_n s + \omega_n^2 = (s + \omega_n)^2 \quad (47)$$

where upon k_{pi} and k_{ii} were obtained as;

$$k_{pi} = kL2\zeta\omega_n - kr_s' \quad (48)$$

$$k_{ii} = kL\omega_n^2 \quad (49)$$

$\zeta$is the damping ratio. ω_n is the natural frequency. The speed control and rotor flux control loops provide the *d* and *q* axis current commands respectively according to equations (18), (22) and (10). PI controllers were also employed for the speed and flux control loops. The block diagram of the speed control system is given in Figure 4 and it is based on the machine dynamics given equation (10).

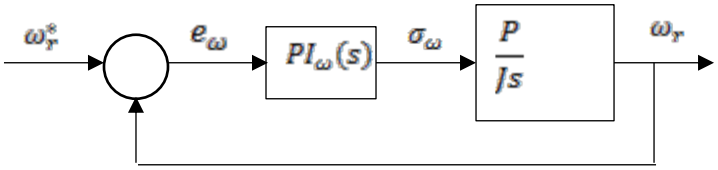

Figure 4: Control Block Diagram for Speed Control

The equation of the transfer function of the speed control loop is obtained from Figure 4 as;

$$\frac{\omega_r}{\omega_r^*} = \frac{k_{pw}s + k_{iw}}{\frac{J}{p}s^2 + sk_{pw} + k_{iw}} \quad (50)$$

The speed controller gains are calculated from (50) as follows;

$$k_{pw} = 2\frac{J}{p}\omega_n \quad (51)$$

$$k_{iw} = \frac{J}{p}\omega_n^2 \quad (52)$$

The control block diagram of the flux control system is obtained from equation (18) and given in Figure 5.

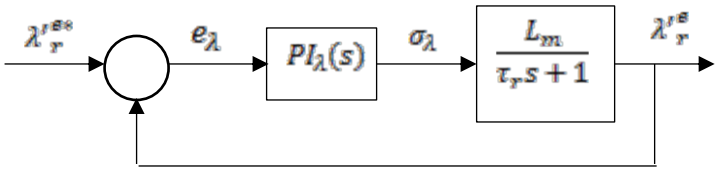

Figure 5: Control Block Diagram for Rotor Flux Control

The equation of the transfer function of the flux control loop is obtained as;

$$\frac{\lambda_r}{\lambda_r^*} = \frac{k_{pf}s + k_{if}}{\frac{\tau_r}{L_m}s^2 + s\left(\frac{1}{L_m} + k_{pf}\right) + k_{if}} \quad (53)$$

The flux controller gains are calculated from equation (53) as follows;

$$k_{pf} = \frac{\tau_r}{L_m}2\omega_n - \frac{1}{L_m} \quad (54)$$

$$k_{if} = \frac{\tau_r}{L_m}\omega_n^2 \quad (55)$$

The supply voltages in the synchronous reference frame are then calculated based on the following equations;

$$V_{qs}^e = \sigma_{qs} + k(\omega_e L i'^e_{ds} + \frac{L_m}{L_r}\omega_r \lambda'^e_r) \quad (56)$$

$$V_{ds}^e = \sigma_{ds} - k\left(\frac{L_m R_r}{L_r^2}\lambda'^e_r + \omega_e L i'^e_{qs}\right) \quad (57)$$

The control objective is to regulate the rotor flux and the torque to their commanded values. Figure 6 shows the block diagram of the rotor flux-oriented optimizing drive scheme for the three-phase induction machine. The inverter supplies the controlled three phase voltages to the three-phase induction motor in such a way that the flux is regulated at its optimum value for each load torque. The torque command is the output of the speed control loop. When the motor drive is in operation, flux is produced in the machine. The flux is controlled to its optimum value by regulating the *d*-axis stator current. This regulation ensures linear control of torque by the *q*-axis stator current. The flux model receives stator currents i_{qs}^e, i_{ds}^e and speed ω_r and delivers the flux $\lambda_r'^{e*}$, supply frequency ω_e and the corresponding angular position θ_e, to ensure proper vector alignment. The block diagram of Figure 6 was implemented in MATLAB/ Simulink.

3. Results and Discussion

In this section, the effectiveness of the proposed method is discussed. Simulation results are presented as well. The motor parameters utilized in order to verify the effectiveness of the proposed scheme are provided in Table 1.

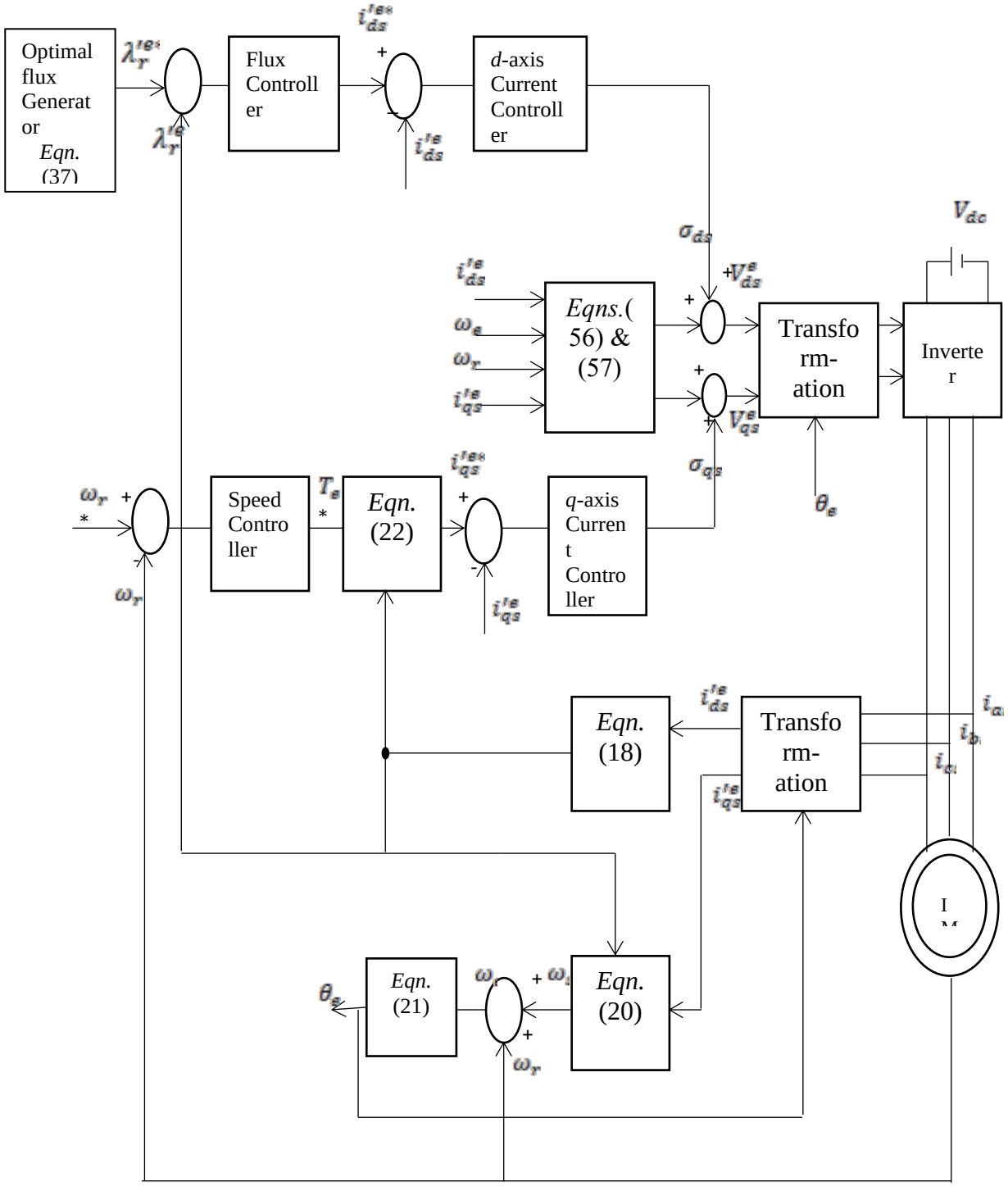

Figure 6: Block diagram of rotor flux oriented optimizing drive

Table 1: Induction Motor Parameters.

Parameter	Value	Parameter	Value
Voltage	400v	R_r	1.52Ω
Frequency	50Hz	R_{fe}	13400Ω
Synchronous speed	3000rpm	$L_s = L_r$	0.2405H
No of poles	2	L_m	0.2323H
Power	3kw	J	0.0044kgm^2
R_s	1.795Ω		

Table 2: Current, speed and flux controller gains

Controller	Proportional gain	Integral gain
q-axis current controller (k_I, k_p)	639.4058	6.3958e+06
d-axis current controller (k_I, k_p)	639.4058	6.3958e+06
Speed controller (k_I, k_p)	1.76	176
Flux controller (k_I, k_p)	268.1424	2.7245e+04

The computed controller gains are as provided in Table 2. The loss minimization algorithm was set to trigger at 2.5s. With the reference speed and load torque set to 250 rad/s and 3Nm respectively, the rated flux was computed as 1Wb. The result of total electrical power loss in the induction motor is presented in Figure 8.

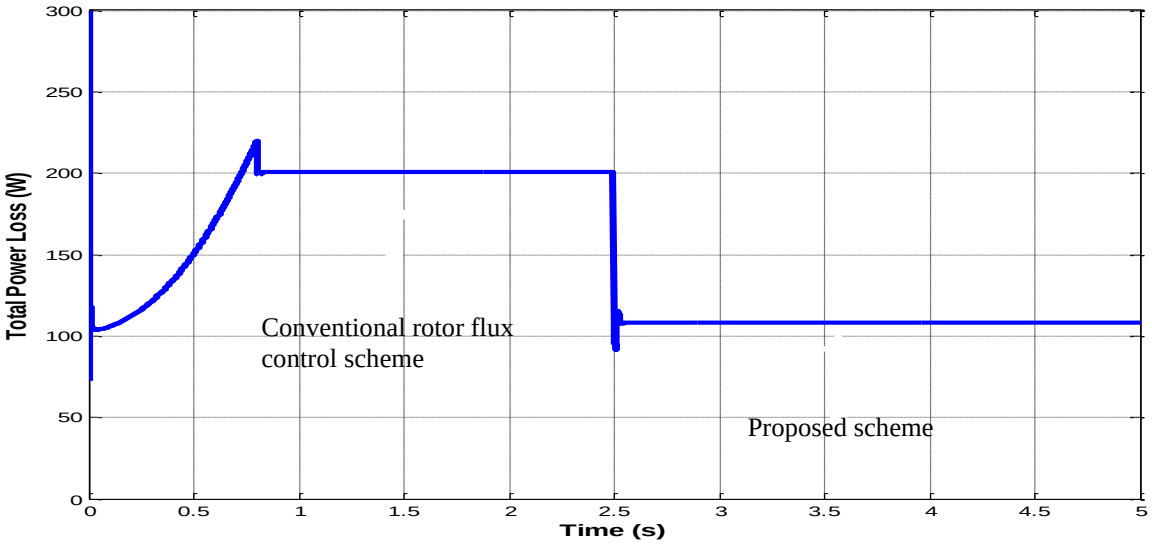

Figure 8: Electrical power loss vs time

It can be seen that the conventional rotor flux control scheme produces a steady state power loss of 200W in the motor. The proposed scheme on the other hand, upon activation at a time of 2.5 s, produces a power loss of 108.04W in the same motor. This gives a significant reduction of 54.02%, the consequence of which is a rise in motor efficiency from 78.9% to 87.41% as shown in Figure 9.

Corresponding author's e-mail address: baolarinoye@abu.edu.ng

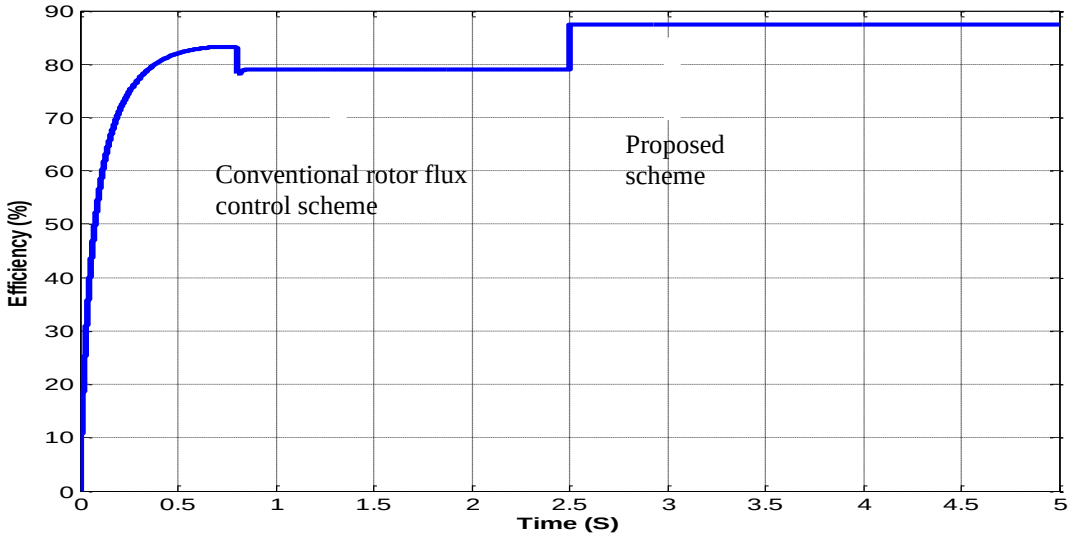

Figure 9: Efficiency of induction motor vs time

Figure 10 shows the plot of the rotor flux magnitude. It can be seen that the flux value is 1Wb until the proposed scheme is activated and the flux reduces significantly to its optimal value of 0.6357Wb for the given load torque. This verifies the analysis set forth, that there is an optimal flux in the motor for which electrical losses are minimized and hence efficiency is maximized for a given load torque.

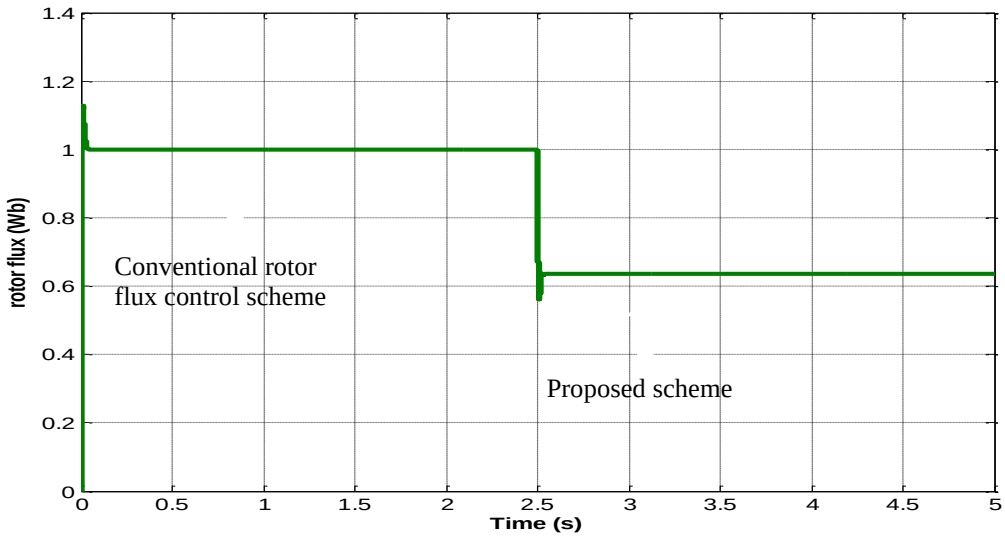

Figure 10: Rotor flux magnitude vs time

Figure 11 shows the speed profile of the induction motor and it can be seen that the motor was set to accelerate and reach a steady state speed of 250 rad/s.

Corresponding author's e-mail address: baolarinoye@abu.edu.ng

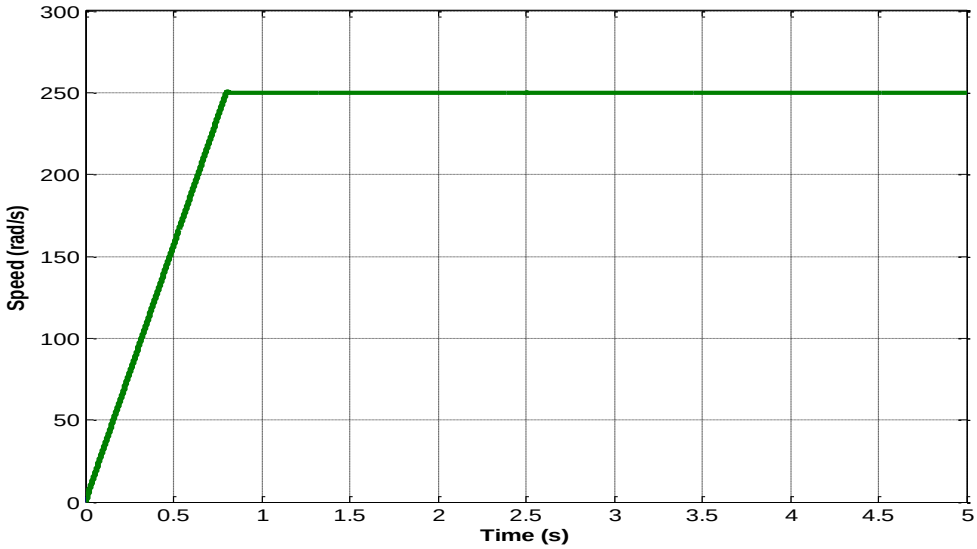

Figure 11: Speed vs time

Figure 12 shows the torque produced in the motor during the simulation time. The steady state torque can be seen to equal 3Nm.

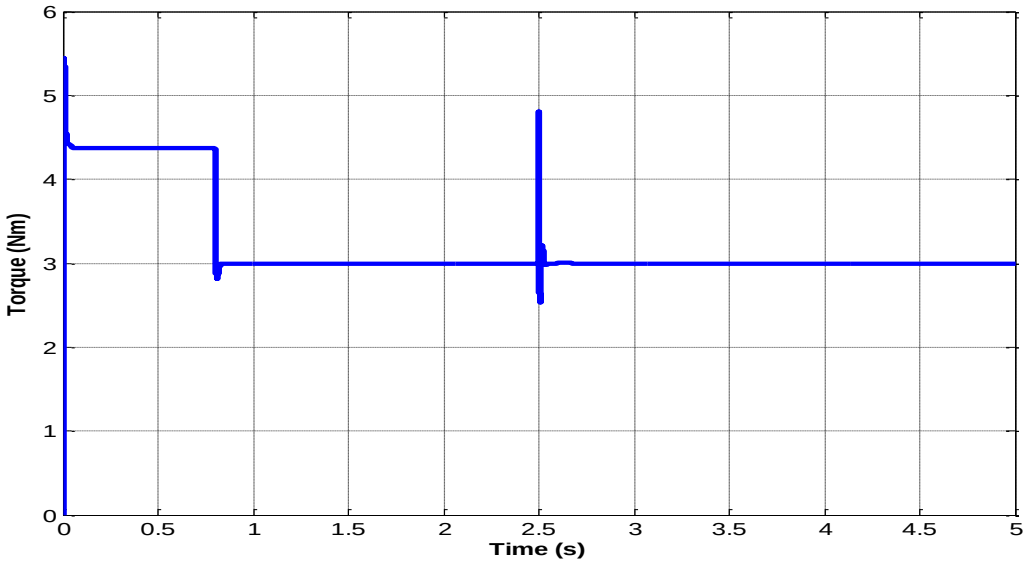

Figure 12: Torque produced vs time

Corresponding author's e-mail address: baolarinoye@abu.edu.ng

Table 3: Comparison of result between conventional, proposed rotor flux control scheme and the conventional and optimized DTC control schemes

Variable	Conventional rotor flux control scheme	Proposed method	Conventional DTC	(Optimized DTC)
Total Power loss (W)	200	108.04	231.1961	166.2806
Efficiency (%)	78.9	87.41	77.1	82.4
Flux (Wb)	1	0.6357	1	0.7539

Table 3 shows a comparison of results between conventional, proposed rotor flux-oriented control scheme and the conventional and optimized DTC control schemes for the same motor parameters, reference speed and load torque. It can be observed that the proposed method gives a superior motor performance. The proposed rotor flux optimization scheme gives 8.51% improvement in efficiency compared to the conventional rotor flux control scheme at a speed of 250rad/s, for a load torque of 3Nm. The proposed scheme also gives a 5.01% improvement in efficiency compare to the optimized DTC control scheme proposed in Aygun & Aktas (2018).

The rotor flux-oriented control scheme enables the variation of motor speed. To this end, the motor speed was ramped down from 250 rad/s to 150 rad/s and allowed to stay at that speed between 4 and 5s of simulation time. Figures 13-15 show the performances of the motor under the proposed scheme at variable speeds.

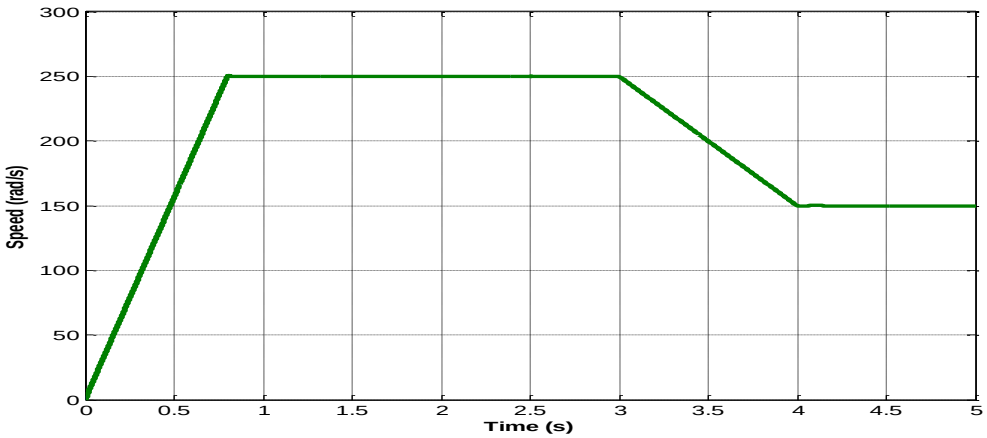

Figure 13: Variable speed profile of the induction motor

The total power loss is plotted in Figure 14 and it can be seen to reduce from 200W to 108.04W as in the previous result but it further reduces to 83.645W because of the drop-in speed. The total power loss therefore reduces by 22.6% and this implies that there is an opportunity to save power when the motor is driven at a lower speed.

Corresponding author's e-mail address: baolarinoye@abu.edu.ng

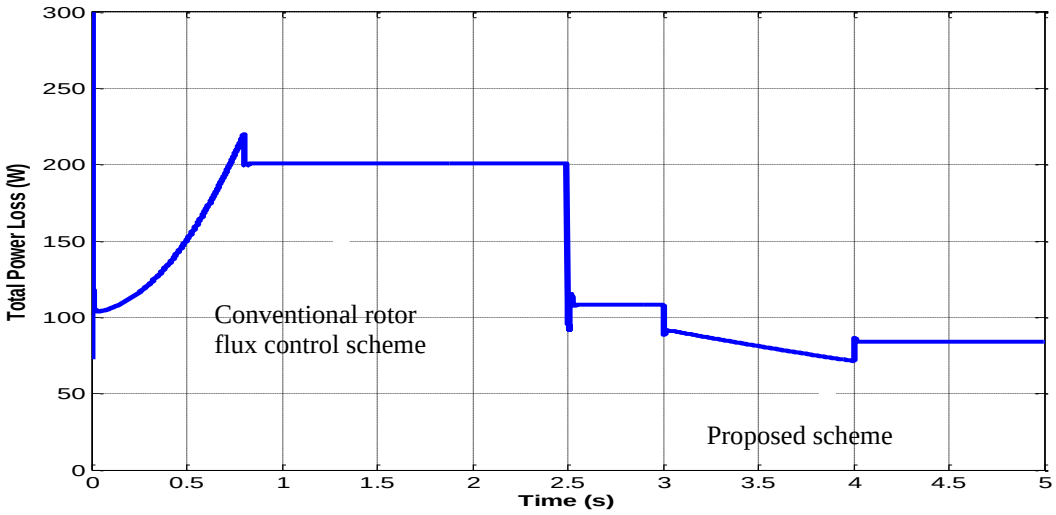

Figure 14: Total electric power loss under under variable speed.

The efficiency of the motor is plotted in Figure 15. It can be seen to decrease to a value of 84.8% after the motor speed is dropped to 150 rad/s because the power output drops with speed. A table of comparison between these results and those obtained in Aygun & Aktas (2018) is provided in Table 4.

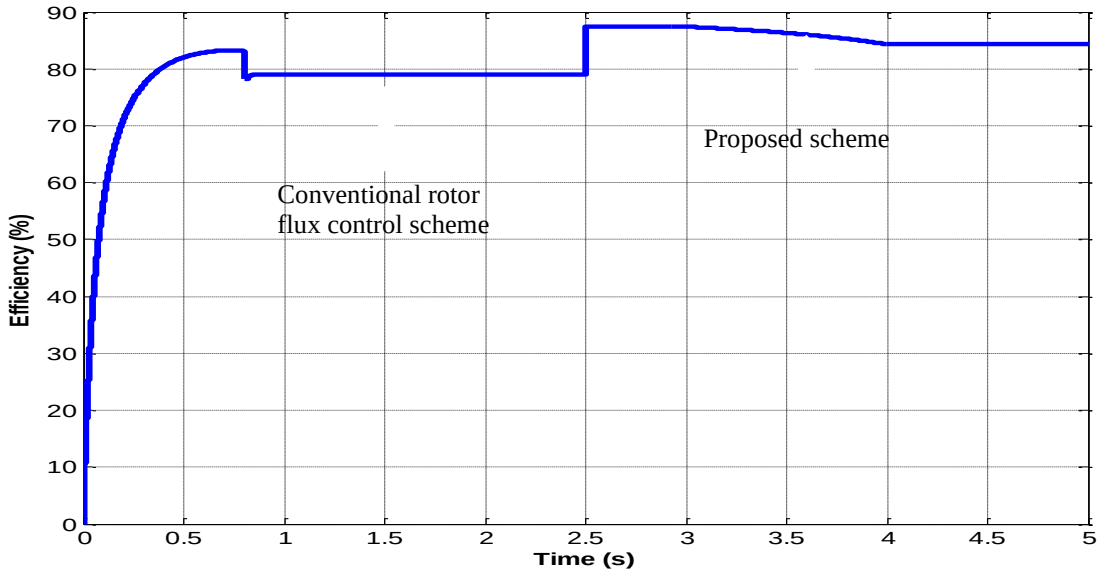

Figure 15: Efficiency of induction motor under variable speed

Table 4: Comparison of results of the proposed rotor flux-oriented control scheme with those of the optimized DTC at variable speed

Scheme	Total power loss (W)	Efficiency (%)
Proposed scheme at 250 rad/s	108.04	87.41
Proposed scheme at 150 rad/s	83.645	84.8
Optimized DTC at 250 rad/s	166.28	82.4
Optimized DTC at 150 rad/s	101	79.1

Table 4 shows the superior performance of the proposed method at variable speed when compared with the performance of the optimized DTC method under the same operating conditions. At a lower speed of 150 rad/s, power loss reduces by 17.2% while efficiency is higher by 5.7% for a load torque of 3Nm under the proposed scheme as compared to the optimized DTC scheme developed in Aygun & Aktas (2018).

Figures 16-20 show the effectiveness of the proposed optimization scheme at varying loads. The load torque on the motor is reduced from 3Nm to 2Nm as shown in Figure 16.

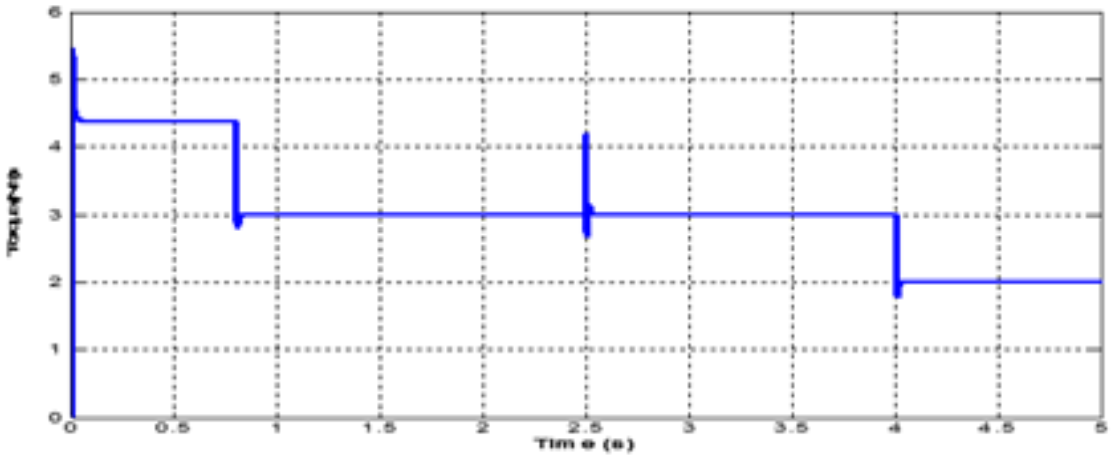

Figure 16: Torque Produced in the motor with load torque varying from 3Nm to 2Nm

In Figure 17, the total power loss is observed to decrease to 72.03 W after the initiation of the loss minimization algorithm because the flux in the motor is optimized for each load torque. The optimal flux for the 2Nm load is 0.5188 Wb as seen in Figure 18. The total loss reduces after the reduction in load from 3Nm to 2Nm because of the reduced output power.

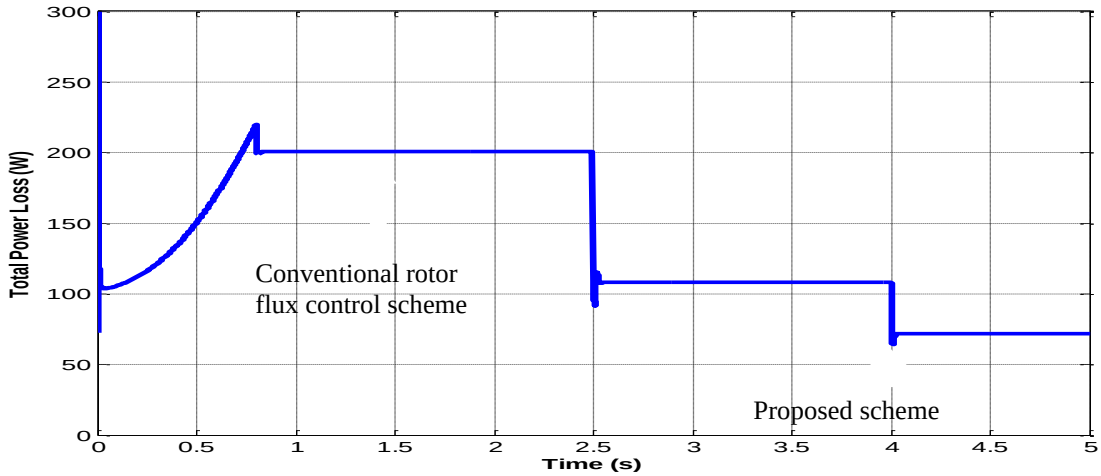

Figure 17: Total power loss with load torques varying from 3Nm to 2Nm

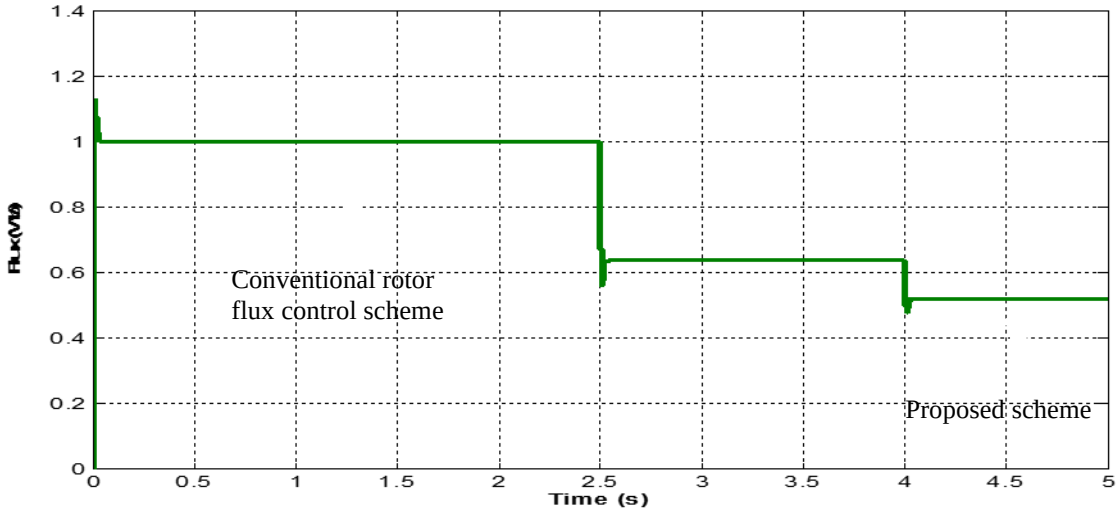

Figure 18: Optimal flux of induction motor with load torque varying from 3Nm to 2Nm

Although the motor operates at a lower load torque, the operating efficiency is observed to be the same as that for the 3Nm load torque. The value is still 87.41% as seen from Figure 19.

Corresponding author's e-mail address: baolarinoye@abu.edu.ng

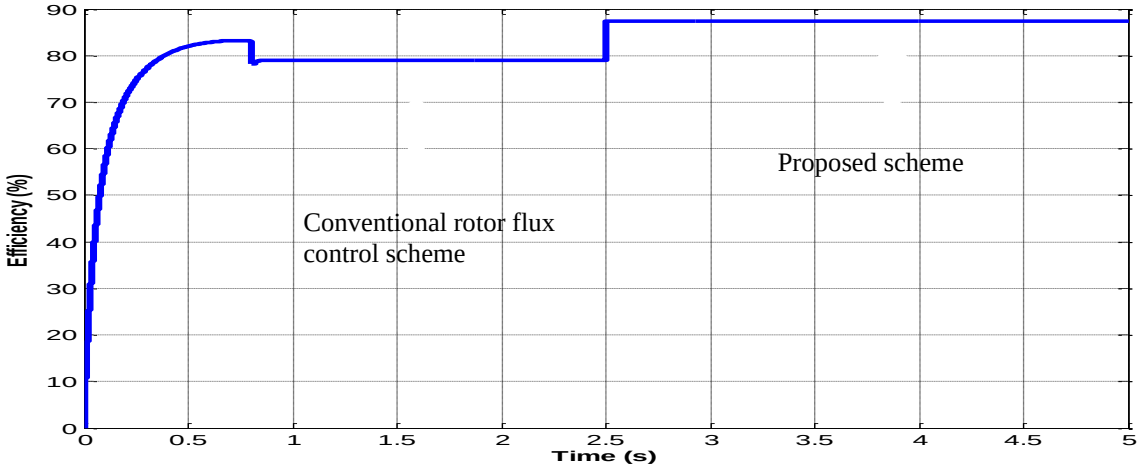

Figure 19: Efficiency of the motor with load torque varying from 3Nm to 2Nm

This implies that the efficiency is maximized for all loads under the scheme. These results follow the same trend as the results provided in Aygun and Aktas (2018). The advantage of the scheme proposed in this paper is that the point of maximum efficiency is higher by 5.01%. Table 5 gives a comparison between the results obtained in this work and those obtained in Aygun and Aktas (2018) when the load torque varied from 3Nm to 2Nm.

Table 5: Comparison of Optimized DTC and Proposed Method at Variable Load.

Scheme	Total power loss (W)	Efficiency (%)
Proposed method at 3Nm	108.04	87.41
Proposed method at 2Nm	72.03	87.41
Optimized DTC at 3Nm	166.28	82.4
Optimized DTC at 2Nm	110.3	82.4

The results suggest that the point of maximum efficiency is independent of the load torque but the optimum flux at which it occurs depends on the load torque. The voltages supplied to the stator windings of the three-phase induction motor are shown in Figure 20.

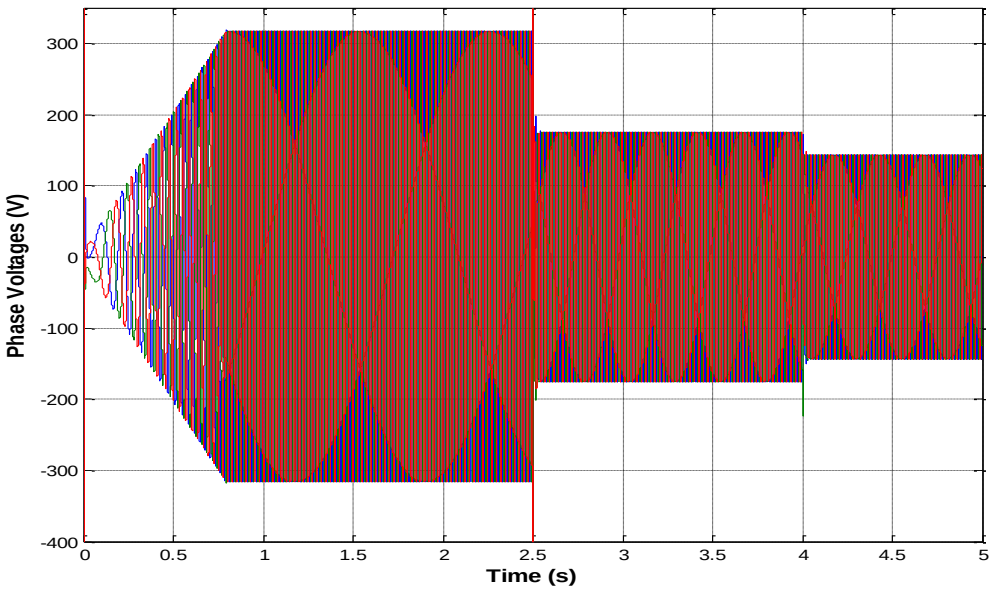

Figure 20: Supply voltages with load torque varying from 3Nm to 2Nm

It can be seen that the magnitude of the stator voltages reduced with load on the machine. This is an energy saving ability of the proposed rotor flux optimization control strategy. The reduction in voltage is a direct result of the reduction in flux to its optimal levels for each load.

Corresponding author's e-mail address: baolarinoye@abu.edu.ng

The magnitude of the stator voltages rises with speed during the time of acceleration of the induction motor. It reaches a value of 311V at steady state while the load torque of 3Nm is applied. The value reduces to 180V after the optimizing control algorithm is activated at 2.5s. The value further reduces to 150V after the load torque changes from 3Nm to 2Nm.

4. Conclusion

A rotor flux optimization control model for a three-phase induction motor was analysed and simulated. A comparison between the conventional and proposed rotor flux-oriented control drive shows that, for a reference speed of 250rad/s and a load torque of 3Nm, the rotor flux reduced from a rated value of 1Wb to an optimal value of 0.6357Wb which invariably led to a significant reduction of the total power loss, in the motor, from 200W to 108.04W and a consequential increase in efficiency from 78.9% to 87.41%. The performance of the scheme at varying load also shows a change in optimum flux from 0.6357Wb to 0.5188Wb after the load torque was reduced from 3Nm to 2Nm. Although the motor operated at a lower load torque, the flux optimization algorithm implemented in MATLAB\Simulink, for the proposed scheme, maintained a maximum efficiency of 87.41%. It was observed that while the point of maximum efficiency is independent of the load torque, the optimum flux at which it occurs depends on the load torque. With the proposed drive scheme operating at variable speed mode in which motor speed was ramped down from 250rad/s to 150rad/s at a load torque of 3Nm, power loss was observed to further reduce significantly by 22.6%. These results suggest that the proposed rotor flux optimization scheme is superior to the optimized DTC scheme proposed in Aygun & Aktas (2018). The proposed scheme also presents an opportunity to save power and therefore energy as the command voltages supplied to the induction motor was observed to decrease with decreasing load applied to the motor.

References

Aygun, H. and Aktas, M. 2018. A novel DTC method with efficiency improvement of IM for EV applications. Engineering, Technology & Applied Science Research, 8(5): 3456-3462.

Chelliah, TR., Yadav, JG., Srivastava, SP. and Agarwal, P. 2009. Optimal energy control of induction motor by hybridization of loss model controller based on Particle Swarm Optimization and search controller. World Congress on Nature & Biologically Inspired Computing, Coimbatore, India, pp. 1178-1183, Doi: 10.1109/NABIC.2009.5393784.

Engel, E., Kovalev, IV. and Karandeev, D. 2015. Energy-saving IOP Conference Series: Materials Science and Engineering, 94: 10. 1088/1757-899X/94/1/012008.

Eseosa, O. and Christian, A. 2018. Energy efficiency optimization of three phase induction motor drives for industrial applications. International Journal of Engineering and Applied Sciences, *5*(8): 42-49.

Faduyile, OE. 2009. Effect of harmonics on the efficiency of a three-phase energy efficient and standard motors. MSc. Thesis. University of Tennessee at Chattanooga. USA.

Kalhoodashti, HE. and Shahbazian, M. 2011. Hybrid speed control of induction motor using PI and fuzzy controller. International Journal of Computer Applications, 30(11): 44-50.

Khan, H., Hussain, S. and Bazaz, MA. 2015. Direct torque control of induction motor drive with flux optimization. In: International Conference on Advances in Computing, Communications and Informatics (ICACCI), IEEE, 618-623.

Laroui, M., Nour, B., Moungla, H., Cherif, MA., Afifi, H. and Guizani, M. 2021. Edge and fog computing for IoT: A survey on current research activities & future directions. Computer Communications, 180(1): 210-231.

Corresponding author's e-mail address: baolarinoye@abu.edu.ng

Lee, PM., Lee, DD., Nguyen, TV. and Nguyen, PH. 2013. Real-time loss minimization control in induction machines based on DSP TMS320LF2812. Science and Technology Development Journal, 16(4): 5-18.

Nam, SW. and Uddin, MN. 2006. Model-based loss minimization control of an induction motor drive. In: IEEE International Symposium on Industrial Electronics, IEEE, 2367-2372.

Olarinoye, GA., Akorede, MF. and Akinropo, CD. 2022. Design and Simulation of a Three-Phase Induction Motor Speed Control System. FUOYE Journal of Engineering and Technology, 7(1): 39 – 46.

Rashtchi, V. and Bizhani, H. 2015. Using of particle swarm optimization for loss minimization of vector-controlled induction motors. Universal Journal of Electrical and Electronic Engineering, 3(3): 71-80.

Sruthi, MP., Nagamani, C. and Ilango, GS. 2017. An improved algorithm for direct computation of optimal voltage and frequency for induction motors. Engineering Science and Technology, an International Journal, 20(5): 1439-1449.

Corresponding author's e-mail address: baolarinoye@abu.edu.ng